Reaction Chemistry & Engineering

Continuous liquid-phase synthesis of nickel phosphide nanoparticles in a helically coiled tube reactor

Journal:	*Reaction Chemistry & Engineering*
Manuscript ID	RE-ART-01-2020-000010.R3
Article Type:	Paper
Date Submitted by the Author:	21-Apr-2020
Complete List of Authors:	Zheng, Huidong; Fuzhou University, Li, Donglin; Fuzhou University, College of Chemical Engineering Chen, Jingjing; Fuzhou University, College of Chemical Engineering Liu, Jie; Fuzhou University, College of Chemical Engineering Yan, Zuoyi; Fuzhou University, College of Chemical Engineering Oyama, S.; Fuzhou University, College of Chemical Engineering; The University of Tokyo, Department of Chemical System Engineering; Virginia Tech, Department of Chemical Engineering

Continuous liquid-phase synthesis of nickel phosphide nanoparticles in a helically coiled tube reactor†

Huidong Zheng,*[a,b] Donglin Li,[a,b] Jingjing Chen,[a,b] JieLiu,[a,b] ZuoyiYan,[a,b] and S. Ted Oyama*[a,b,c,d]

ABSTRACT: The continuous liquid phase synthesis of nickel phosphide (Ni_2P) nanoparticles was studied in a helically coiled tube (HCT) reactor both in single-phase and two-phases slug flow. The reactants were nickel acetylacetonate, tri-*n*-octylphosphine (TOP) in a 1-octadecane solvent. For the single-phase mode, various parameters such as reaction temperature, residence time, TOP concentration, and P/Ni ratio were studied. It was found that lower temperatures of 320 and 340 ^oC resulted in the formation of mixed $Ni_{12}P_5$ and Ni_2P phases, while a higher temperature of 360 ^oC gave mostly Ni_2P, with particles sizes increasing from 28to 42 nm. Upon varying the contact time between 88~340s at 360 ^oC, a likely sequence of reaction involved an amorphous phase that was transformed in parallel to Ni, $Ni_{12}P_5$, and Ni_2P. When the flow in the HCT was changed to two-phases slug flow by using N_2 to split continuous liquid phase into small liquid columns, the product was nearly 100% Ni_2P and the particle size was as small as 3-4 nm. This was attributed to enhanced mass transfer in the small liquid columns of the slug flow that led to higher reaction rates. It is highlighted that HCT operated at slug flow is an efficient and continuous method for the fabrication of nanoparticles.

[a] Fujian Engineering Research Center of Advanced Manufacturing Technology for Specialty Chemicals & Fujian Key Laboratory of Advanced Manufacturing Technology for Specialty Chemicals, College of Chemical Engineering, Fuzhou University, Fuzhou, Fujian 350108, P. R. China. *E-mail: youngman@fzu.edu.cn
[b] Fujian Science & Technology Innovation Laboratory for Chemical Engineering of China, Quanzhou, Fujian 362114, P. R. China.
[c]Department of Chemical System Engineering, The University of Tokyo, 7-3-1 Hongo, Bunkyo-ku, Tokyo 113-8656, Japan. *E-mail: oyama@vt.edu
[d] Department of Chemical Engineering, Virginia Tech, Blacksburg, Virginia, 24060, USA
† Electronic Supplementary Information (ESI) available: [details of any supplementary information available should be included here]. See DOI: 10.1039/x0xx00000x

1. Introduction

Many types of reactors are now used in the traditional chemical industry. These may be broadly classified as backed-mixed, of which batch and continuous stirred-tank reactors (CSTRs) are emblematic, and segregated, of which plug-flow reactors (PFRs) are stereotypical, such as helically coiled tube reactor (HCT). One disadvantage of CSTRs is that they provide a broad distribution of residence times, while PFRs can give a narrow contact time. As well known, precisely short reaction time is favorable for controlling the growth process of nanoparticles. In order to obtain monodisperse nanomaterials, it is desirable to provide a uniform reaction environment and stable operating conditions such as pressure, temperature, and concentration. In these aspects, millifluidic reactors exhibit excellent performance. Millifluidic reactors provide for thermal and chemical homogeneity in the reaction volume because of their small dimensions.[1,2]Moreover, the reactants are highly dispersed in the reactor, which can prevent the local supersaturation of the reactants, make the nucleation and growth of the particles uniform, and avoid agglomeration. HCT is the simplest type of millifluidic reactor. Rippel et al.[3] have presented correlations of pressure drop and axial dispersion based on tracer methods for HCT reactors, and classified different flow regimes as bubble, slug, stratified, wavy, semi annular, and annular. In slug flow, where the liquid phase is held in a restricted volume, there is increased heat transfer, and diminished internal concentration gradients through internal convection.[4]So HCT can also provide a uniform temperature and concentration field for the reaction system, which is exactly required for nanoparticle growth. Millifluidic reactors (reactors with channel dimensions of 0.5–10.0 mm) are gaining popularity in nanoparticles synthesis because of many of the same synthetic advantages as microfluidic devices, but are simpler to construct, easier to reconfigure, and more straightforward to interface with in situ monitoring techniques.[5] There have been a number of reports on the successful use of millifluidic reactors to prepare nanoparticles. For example, Lohse et al.[6] have demonstrate the construction and operation of a simple millifluidic reactor and it can synthesize gold nanospheres with strictly controlled diameters and gold nanorods with controlled length-to-diameter ratios between 1.5 and 4.0. Biswas et al.[7] used millifluidic reactor to significantly shorten the residence time and residence time distribution, and realized the continuous flow synthesis of ultrafine copper nanoclusters with excellent colloidal stability. Although there has been a significant amount of work on the synthesis of nanoparticles in liquid single-phase and liquid-liquid two-phases systems[8-10], little work has been done investigating nanoparticle synthesis in gas-liquid two-phases media.[11,12]

As a new material, Ni_2P is widely studied[13, 14]an anti-corrosion, anti-wear and waterproofing material[15,16], and has promising application prospects in the field of luminescent devices, electronic components and magnetic elements.[17] Besides, Ni_2P is also a promising catalytic material[18]. Oyama and co-workers[19] synthesized the transition metal phosphides Ni_2P, Co_2P, MoP and Fe_2P, and studied their catalytic performance in the hydrodeoxygenation of the biomass model compound 2-methyltetrahydrofuran, and found that Ni_2P was the most active. Typically, the Ni_2P catalyst was prepared by a gas-solid phase method, i.e., temperature-programmed

reduction (TPR).[20-22]Zhang et al.[23]have also done similar work and prepared hollow nanoparticles with diameters of about 20–80 nm. However, the crystal phase, morphology and particle size are difficult to control with TPR. Another way to prepare Ni_2P nanomaterials is liquid phase synthesis such as water/solvothermal,[24, 25] organometallic phosphating,[26, 27-29] and milli-emulsion methods.[30] In these liquid-phase methods, nickel phosphide nanoparticles are synthesized in a batch reactor using tri-*n*-octylphosphine (TOP) as the source of phosphorus. In the presence of TOP, nickel phosphide nanoparticles of different phase are formed, whose properties depend on the temperature, flow rate, residence time and molar ratio of Ni/P.[28] Habas et al.[31] have prepared phase-pure Ni_2P nanoparticles in a one-pot reaction. The method provides controlled phases and avoids the formation of unwanted hollow particles. Zhang et al.[32] have also studied the "one-step" liquid phase synthesis of Ni_2P nanoparticles in batch reactors and applied the material as a catalyst in the hydrodeoxygenation of 2-methylfuran. The liquid phase method is simple because the conditions can be easily controlled. However, in most cases, it is difficult to obtain phase-pure Ni_2P product in batch reactors, and other phases such as $Ni_{12}P_5$ and Ni_5P_4 are hard to avoid because these three phases are formed in a narrow temperature range (300~350^{o}C).[33] Control of the Ni_2P nanoparticle size can also be challenging since varying the reaction parameters such as temperature, precursor ratio (P/Ni), surfactant concentration, and heating time may lead to morphological and phase changes in the nickel phosphide systems.[34]Another disadvantage of the batch method is that it is not beneficial to scale up production because of the amplification effect.

Based on the previous work done by Zhang et al.[32], HCT can be applied to the continuous preparation of nanoparticles by liquid phase method. In the present study the synthesis of nickel phosphide nanoparticles is carried out in a continuous HCT reactor using nickel acetylacetonate and TOP dissolved in 1-octadecene as reactants. The influence of synthesis parameters such as temperature, TOP concentration, P/Ni ratio, and total flow is investigated. Besides, nickel phosphide nanoparticles were also synthesized in a two-phases slug flow by adding a gas phase of nitrogen to the reactants. It is found that the nickel phosphide nanoparticles produced in the slug flow are relatively uniform, small-sized, and phase-pure as compared to those obtained in the continuous flow. This preparation method can be extended to the continuous preparation of other nanoparticles.

2. Experimental section

2.1. Chemicals and Reagents.

Nickel acetylacetonate (95%), 1-octadecene (>90%;ρ = 0.78 g/cm^3) and tri-*n*-octylphosphine (TOP;90%; ρ = 0.83g/cm^3) were purchased from Sigma-Aldrich, and the tri-*n*-octylphosphine was stored under vacuum. Chloroform (99.5%) was purchased from Xilong Scientific, and ethanol (99.5%) was purchased from Sinopharm Chemical Reagent Co., Ltd. All chemicals were used as received.

The reagent mixture for the synthesis was obtained by uniformly mixing 1.0 mmol nickel acetylacetonate ($Ni(acac)_2$, 0.27 g) and 16 mmol TOP (8.0 mL) under stirring at room temperature, and then adding 33mmol 1-octadecene (12.0 mL) as a diluent. The

concentrations of each component are calculated by Equation(S1-1)and the concentration for $Ni(acac)_2$,TOP and 1-octadeceneare represented by C_{Ni}, C_{TOP}, and $C_{1\text{-}oct}$, respectively.(C_{Ni}= 0.05M; C_{TOP}= 0.80M; $C_{1\text{-}oct}$= 1.70 M)The mixture was subsequently placed in a 70 ^{o}C ultrasound bath for 10 min. It was observed that the color of the mixture changed from light green to dark green.

2.2. Flow synthesis of nickel phosphide nanoparticles.

Figure 1 shows a schematic diagram of the reactor system used in the preparation of the nickel phosphide nanoparticles. The system could be employed in two modes, single-phase and two-phases flow. The single-phase reactor did not utilize N_2 gas in the feed. The two-phases flow comprised four parts. First, a syringe pump with a 27-gauge stainless steel needle allowed delivery of the reagent mixture at a constant flow rate of 1.0 mL/min. (Sometimes at 0.5 mL/min for the two-phases flow mode.) Second, a T-junction(Swagelok, SS-200-3), which is used to connect the pump, gas mass flow controller and reactor though one 316 SS Nut, 1 front ferrule and 1 back ferrule respectively that broke up the flow into a series of small volumes by continuously adding N_2gas to the liquid stream and generated slug flow in the flow channel. N_2 was introduced by a gas mass flow controller (MFC) at a flow rate of 0.5-1.0 mL/min. Third, two coiled stainless steel tubular sections comprising a preheating zone and a reactor zone were used for the synthesis reaction. The preheating section (inner diameter d = 2.0 mm; the pitch of the helix: 2 mm; the diameter of the helix: 30 mm) was immersed in an oil bath kept at 70-100 ^{o}C. The reaction section (d = 1.0 mm; the pitch of the helix: 2 mm; the diameter of the helix: 20 mm) was placed in an oil bath held between 320 and 360 ^{o}C. Three tubing lengths (2.3, 4.5, and 9.0 m) were used to control the residence time of the reactor while keeping the total flow rate constant. Taking the thermal expansion of the flow into account, the residence time τ can be calculated as Equation (S2-1, S2-2).For a liquid flow rate of L = 1.0 mL/min and a reaction temperature of T = 360 ^{o}C, tube lengths of 2.3, 4.5, and 9.0 m gave residence times of 88, 170, and 340 s for the single-phase process, respectively. Fourth, a round-bottom flask kept in a 50 ^{o}C water bath was used to collect the reaction products every 0.5 h. Details are presented in the next section. In millifluidicreactions, it is generally assumed that the system will reach steady state after two residence times.[35] So in order to be representative and reproducible, the product was received after two residence times in the experimental operation, and the whole system runs for at least 8 times of the residence time.

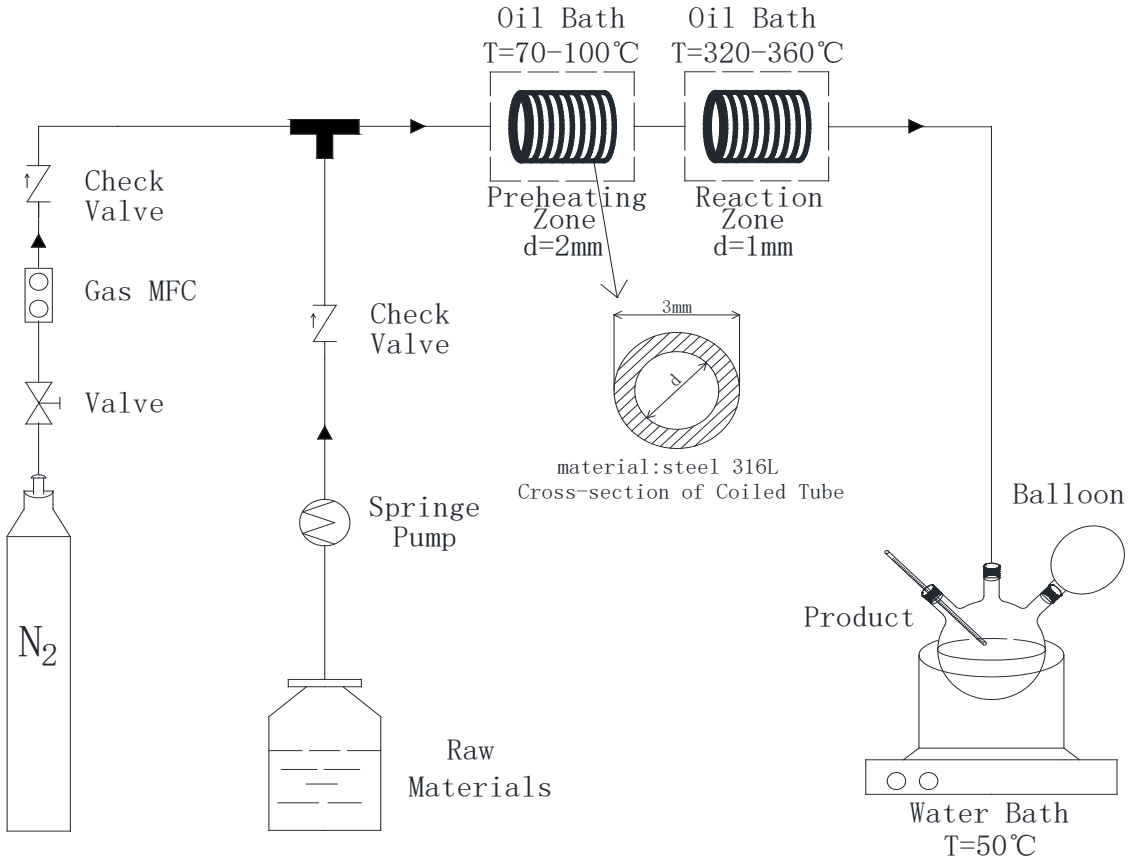

Figure1. Schematic of the experimental setup for the two-phases slug flow synthesis of nickel phosphide nanoparticles.

2.3. Visualization of gas-liquid two-phases in HCT.

Before the two-phases flow synthesis, the visualization of gas-liquid two-phases in HCT in which the continuous flow in the previous measurements is broken up by the introduction of N_2 gas in a T-mixer. The inner diameter of the tube *d* is 1.0 mm, the same as in the HCT used in the syntheses. The measurements were carried out at room temperature, the same temperature at which the T-junction was maintained in the synthesis apparatus, but it is expected that the slug flow regime will persist at reaction temperatures. The photo of a mock set-up designed entirely to observe the slug flow. And the material of tube is PFA while the length is 4.5 m. But the set-up used to synthesize Ni_2P is the same as in Figure 1.

2.4. Nanoparticle washing.

After 0.5 h of product collection in the chilled flask, 10 mL chloroform was added to the contents while stirring, and then 20 mL ethanol was added to precipitate the particles with stirring for 30 min. Then the flask contents were split into two 50 mL centrifuge tubes and were centrifuged at 8000 rpm for 10 min in an Eppendorf 5702 centrifuge. The brown supernatant was removed, and the black precipitate (as-prepared Ni_2P) was dispersed into 10 mL chloroform in an ultrasonic bath for 10 min to remove organics bound to the surface of the nanoparticles. Then 20 mL ethanol was added and the material was again centrifuged. The centrifugation and washing steps were repeated

three times. After the last centrifugation, the supernatant was decanted and the tubes were placed in an 80 ^{o}C drying oven under vacuum to evaporate any remaining liquid. The product yield was calculated from the ratio of Ni_2P product collected to the theoretical amount of Ni_2P product expected from the fed reagents. The formula is shown in ESI (S2-3).

2.5. Characterization of nickel phosphide nanoparticles.

Images of the nickel phosphide nanoparticles were taken using a Nova NanoSEM 230 field scanning electron microscope (SEM) using the in-beam secondary electron detector at an accelerating voltage of 15.0 kV. The samples were first dispersed in chloroform with an ultrasonic bath and deposited on conductive adhesive tape. Before transferring into the SEM instrument, the samples were sputter-coated with a gold-palladium layer to improve conductivity. Size measurements were done by importing the SEM micrographs into the software NanoMeasurer 1.2.

Transmission electron microscopy (TEM) was performed using a TECNAI G2 F20 electron microscope operating at a voltage of 200 kV. Samples for TEM were prepared by dispersing Ni_2P nanoparticles in chloroform. A drop of the resultant solution was deposited on a carbon-coated 200 mesh Cu grid (SPI), followed by air drying for a few minutes. The TEM images were analyzed by Nano Measurer 1.2. Nanoparticles with clear edges were manually selected from different regions of the micrograph, and the longest axis of each particle were measured and recorded as the particle size. The particle size distribution, mean size, and standard deviation were calculated by accounting 100 nanoparticles.

X-ray diffraction (XRD) of the nanoparticle samples was conducted on a DY1602/Empyrean diffractometer. The diffractometer was equipped with a copper X-ray tube, and Cu Kα X-rays were used for the analysis (λ=0.154178 nm). The tube was operated at a voltage of 40 kV and a current of 100 mA. Samples were deposited on a zero-background quartz holder with a groove, and the data were acquired in the 2θrange of 20-80^{o} with a step size of 2.0^{o}.The crystal size was calculated by Scherrer equation:

$$D=\frac{K\lambda}{\beta\cos\theta} \quad (1)$$

where the shape factor K=0.9, β is the full width at half maximum of the diffraction peak, and θ is the Bragg diffraction angle.

3. Results and discussion

3.1. Single-phase flow synthesis.

The Reynolds number at the conditions of this study is 100-250, so the flow regime is in the laminar region. At continuous conditions this will lead to a parabolic profile and uneven concentration distribution of the liquid phase in the tube, and the size of the formed nanoparticles will not be uniform.[36] In the following sections, the effect of changing reaction temperature, reactant concentrations, and residence time are studied on the size, shape, and particle size distribution of the synthesized nanoparticles.

3.1.1. Effect of reaction temperature.

The reaction temperature is an important factor which directly affects the rates of nucleation and growth of nanoparticles. The reaction temperature directly affects both the rate of mass transfer from the bulk phase and the synthesis kinetics. One of the advantages of the tubular reactor is that it has excellent heat transfer performance and can provide a uniform temperature field for the reaction system to control the growth of nanoparticles. According to the conclusions of other research groups, the preferred synthesis temperature for Ni_2P nanoparticles is between 320-350 ^oC,[32] so in this study three temperatures were investigated: 320,340 and 360^{o}C.A temperature of 380 ^{o}C was also examined but it was found that TOP and 1-octadecene were vaporized at this temperature and the synthesis could not be carried out. In the experiments, the total liquid flow rate L was 1.0 mL/min and the residence time τwas170 s. The difference of residence time between each temperature caused by the thermal expansion of liquid was about 2 s, which was negligible compared to the average residence time of 170 s.

Figure 2 shows the XRD patterns of the synthesized nickel phosphide at different synthesis temperature. The diffraction peaks at 2θ = 40.5^o, 44.2^o, 46.8^o and 54.0^{o}can be assigned to Ni_2P (hexagonal, PDF 74-1385). Other peaks at 2θ = 38.4^o and 49.0^o appear exclusively in $Ni_{12}P_5$ (tetragonal, PDF 74-1381). With increasing temperature, the $Ni_{12}P_5$ phase is less observed and the Ni_2P phase becomes predominant. The crystallite sizes of indicated in Figure 2 are for Ni_2P and were obtained from the Scherrer equation assuming a shape factor of 0.9. The full-width at half-maximum was obtained for the peak at 2θ = 40.5^o because it was of high intensity and did not overlap with the peaks of $Ni_{12}P_5$. It should be noted that for these XRD patterns there is a broad, curved background (indicated by the dotted lines underneath each pattern) that suggest there is an amorphous component in the product. Also, the diffraction lines appear to be composed of a sharp component and a diffuse part, indicative of different crystallinities. This will be discussed later. Overall, from these results it can be concluded that 360 ^{o}C is better for the continuous synthesis of the Ni_2P nanoparticles.

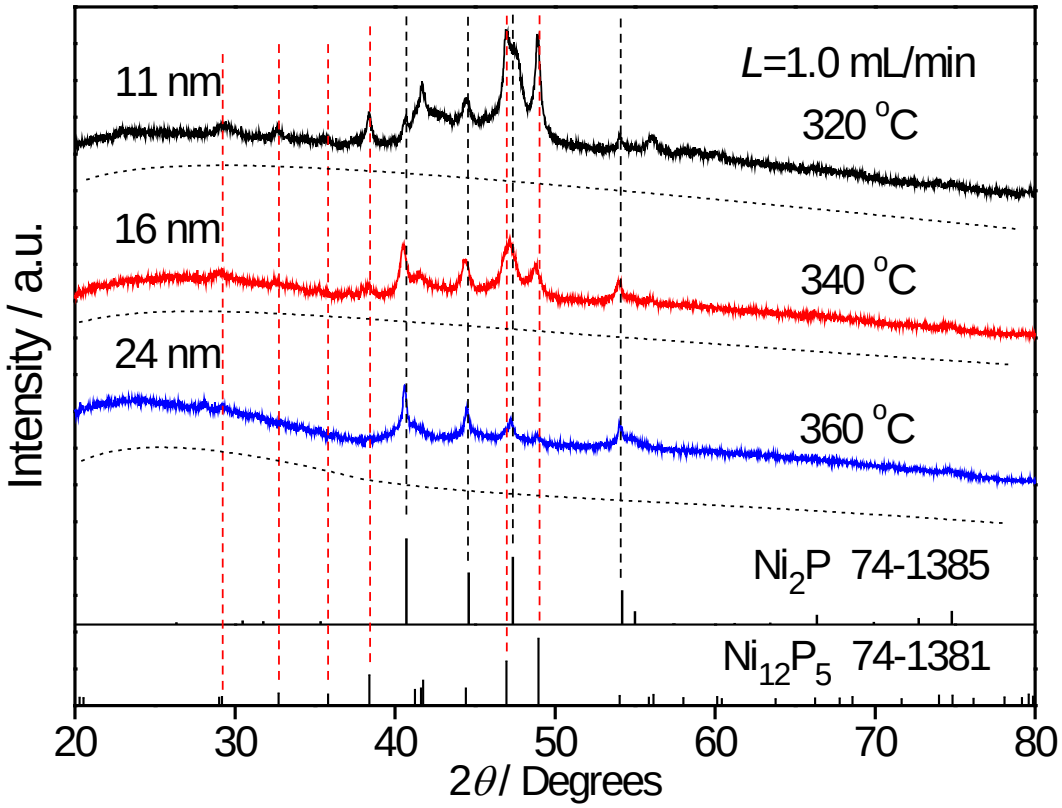

Figure 2.XRD patterns of Ni_2P nanoparticles synthesized at reaction temperatures 320,340, and 360°C; τ= 170s;C_{Ni} = 0.05 M;C_{TOP} = 0.80 M;$C_{1\text{-}oct}$ = 1.70M.Reference patterns are also displayed (Ni_2P PDF # 74-1385; $Ni_{12}P_5$ PDF # 74-1381).

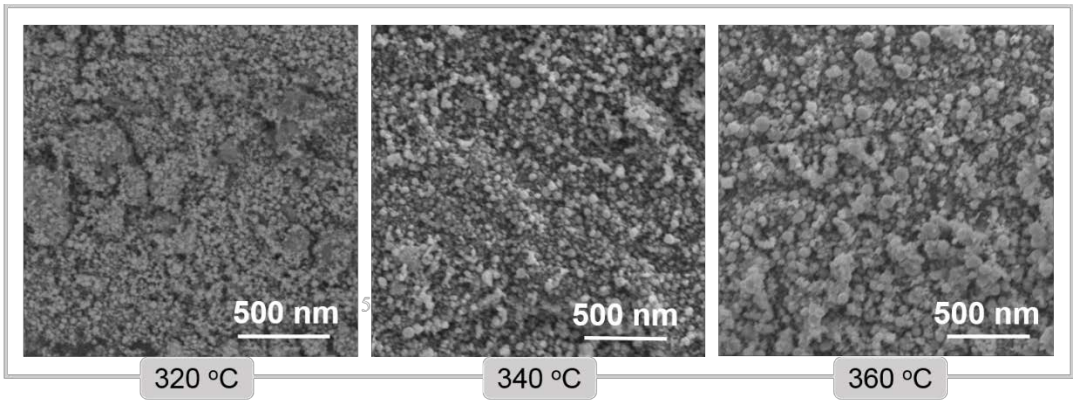

Figure 3. Scanning electron micrographs of Ni_2P nanoparticles synthesized at reaction temperatures 320, 340, and 360 °C; τ= 170 s; C_{Ni} = 0.05 M; C_{TOP} = 0.80 M; $C_{1\text{-}oct}$ = 1.70 M.

Figure 3 shows SEM micrographs of the nanoparticles prepared at different temperature and Figure S1 shows the size distribution of the particles as measured by Nano Measurer 1.2. It can be seen that the prepared particles are spherical and are uniform. They grow in size with increasing temperature from 28 to 42 nm (Figure S3).This is because the growth rate of nanoparticles rises with increasing temperature.

3.1.2. Effect of residence time.

The effect of residence time was investigated at a constant total flow rate of 1.0 mL/min by using three different reactor lengths. Figure 4 shows the effect of changing residence time on the crystallization and particle size calculated by the Scherrer equation for a reaction temperature of 360 °C, a bulk phase $Ni(acac)_2$ concentration of 0.05 M, and a TOP concentration of 0.80 M.

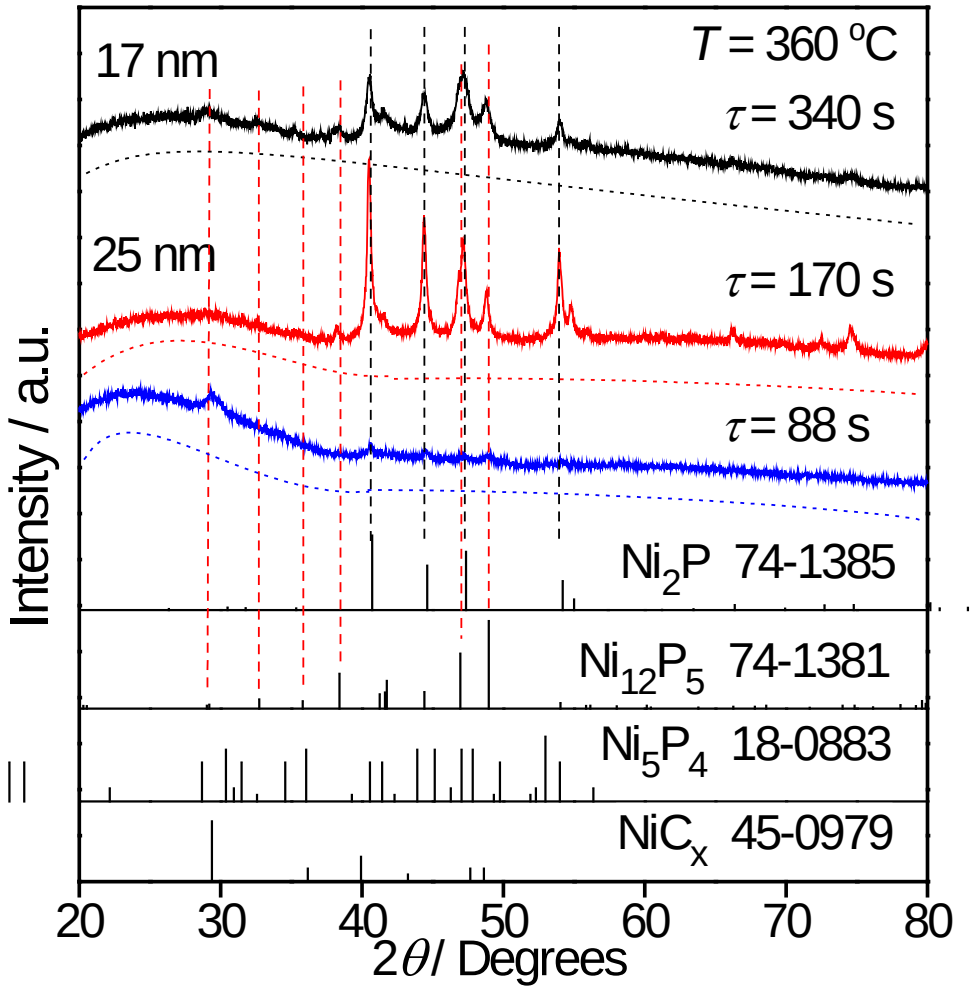

Figure 4. XRD patterns of Ni_2P nanoparticles synthesized with residence times of 88, 170 and 340 s; T = 360 °C; L = 1.0 mL/min; C_{Ni} = 0.05 M;C_{TOP} = 0.80 M;$C_{1\text{-}oct}$ = 1.70 M. Reference patterns are also displayed (Ni_2P PDF # 74-1385; $Ni_{12}P_5$ PDF # 74-1381; Ni_5P_4 PDF # 18-0883; NiC_x PDF # 45-0979).

As the residence time increases from 88 to 170 s, the crystallinity increases significantly. As the residence time increases from 170 to 340 s, the calculated particle size decreases from 25 to 17 nm. Moreover, the amorphous background (dotted curve below each pattern), is substantial at 88 s, but decreases for 170 and 340 s. This is evidence for the existence of an amorphous phase (AP) in the early stages of synthesis. It can be seen from Figure 4that when the residence time is 88 s, small diffraction peaks for Ni_2P appear. This is because the residence time is too short and the materials flow out of the reactor before the Ni_2P crystals can grow. The peak at around 29° is likely

due to the (211) and (220) peaks of $Ni_{12}P_5$, with only these low angle peaks appearing and slightly shifted because of the small size of the diffraction domain. It is also possibly the (111) peak of NiC_x (PDF # 45-0979), with the carbon derived from residual solvent or TOP, although another reduced form is possible. This will be denoted as Ni in the ensuing discussion. The peaks for Ni_2P are displaced to lower angle from the reference, indicating an larger lattice spacing. It should be noted here that the crystal phase obtained from the XRD pattern is impure, which is due to the interruption of the reaction sequence at an intermediate stage. As for the residence time of 170 s, the major phase of the product now is apparently Ni_2P, with little $Ni_{12}P_5$ (38.4 °, 41.6 ° and49.0 °) and Ni_5P_4 (31.5 ° and 32.6 °) in it. When the residence time is 340 s, the major phase is still Ni_2P, and the $Ni_{12}P_5$ (29.0 °, 29.1° (shifted), 32.7 °, 35.8 °,38.4 °, 49.0 °and56.0 °), Ni_5P_4 (22.3 °, 32.6° and 41.5°).As the other major characteristic peaks of Ni_5P_4 (30.1 °, 36.1 °, 47.9 °, 53.1 °) did not appear in Figure 4, this indicates that the content of Ni_5P_4isvery low in the sample.

As shown in Table 1 the content of $Ni_{12}P_5$ rises with increase of residence time, while the content of Ni_2P increases at first and then decreases. This may be because the $Ni_{12}P_5$ phase is formed from the AP, increasing its relative proportion. The amorphous background is visible in all three XRD patterns in Figure 4, but decreasing with increasing residence time. Overall, the results are consistent with the growth mechanism of Ni_2P particles in the synthesis process to be as shown below.

Table 1. Mass percent of various phases.

τ /s	Ni_2P/wt%[a]	$Ni_{12}P_5$/wt%	Ni / wt%
88	49	14	37
170	72	28	-
340	60	40	-

[a] determined by the data in Figure 4.

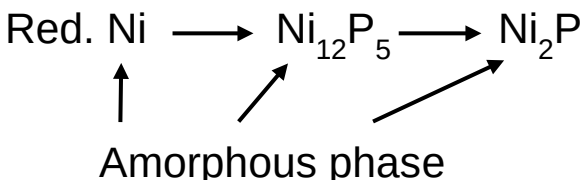

Scheme 1. Reaction sequence for synthesis of nickel phosphide.

Thus, the situation is a bit more complicated than suggested earlier.[37] It is expected that the ultimate product will be Ni_2P at high reaction extents.

3.1.3. Effect of TOP concentration.

Figure 5shows the effect of varying the concentration of the TOP solution in the liquid phase from0.60 M to 1.00 M at a reaction temperature of 360 °C and a bulk phase $Ni(acac)_2$ concentration of 0.05 M. In the experiments, the total flow rate *L*was1.0 mL/min and the residence time τ was 170s. The initial amounts of each material added

in experiments are shown in Table 2.

Table 2. The amount of raw materials for preparing different concentrations of TOP.

n_{Ni}/mmol	n_{TOP} / mmol	$n_{1\text{-}oct}$/mmol	C_{TOP}/M
1.0	12	39	0.60
1.0	16	33	0.80
1.0	20	27	1.00

The increase of TOP from 0.60 M to 1.00 M had little effect on particle size, which was 46-48 nm (Figures S4and S5, the data of particle size distribution from software NanoMeasurer 1.2). As can be seen from Figure 5, when the concentration of TOP was 0.60 M, there was only Ni_2P in the product. As the concentration of TOP increased from 0.60 M to 1.00 M, the amount of $Ni_{12}P_5$ in the product also grew. This may have been due to the transformation of the amorphous phase to $Ni_{12}P_5$. The TOP concentration of 0.80 M and 1.00 M produce very similar morphologies, which could be found in the SEM micrographs in Figure S4.

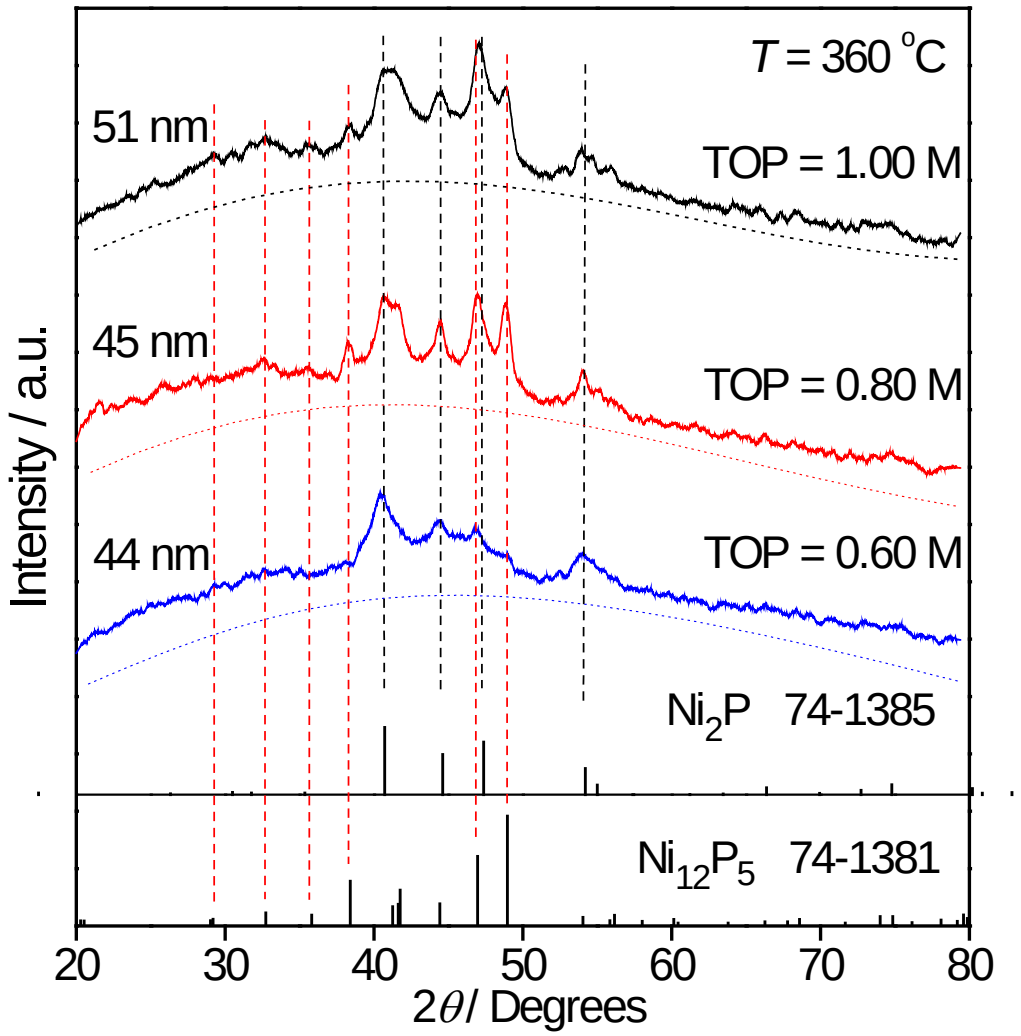

Figure 5. XRD patterns of Ni_2P nanoparticles synthesized with TOP concentrations of 0.60, 0.80

and 1.00 M;T = 360 °C; L = 1.0 mL/min; τ= 170 s; P/Ni = 16.0;C_{Ni}= 0.05 M. Reference patterns are also displayed (Ni_2P PDF # 74-1385; $Ni_{12}P_5$ PDF # 74-1381).

3.1.4. Effect of the ratio of P/Ni.

In addition to temperature, residence time, and TOP concentration, the P/Ni ratio is also an important parameter affecting the formation of Ni_2P nanoparticles. Figure 6shows XRD patterns obtained by varying the P/Ni ratio by changing the amount of TOP added. In the experiments, the total liquid flow rate L was 1.0 mL/min, the residence time τ was 170 s and the reaction temperature T was 360 °C. In the experiments, the dosages of $Ni(acac)_2$ (1 mmol) and 1-octadecene (33 mmol) were constant, and TOP amounts of 2-16 mmol were added to achieve different P/Ni ratios.

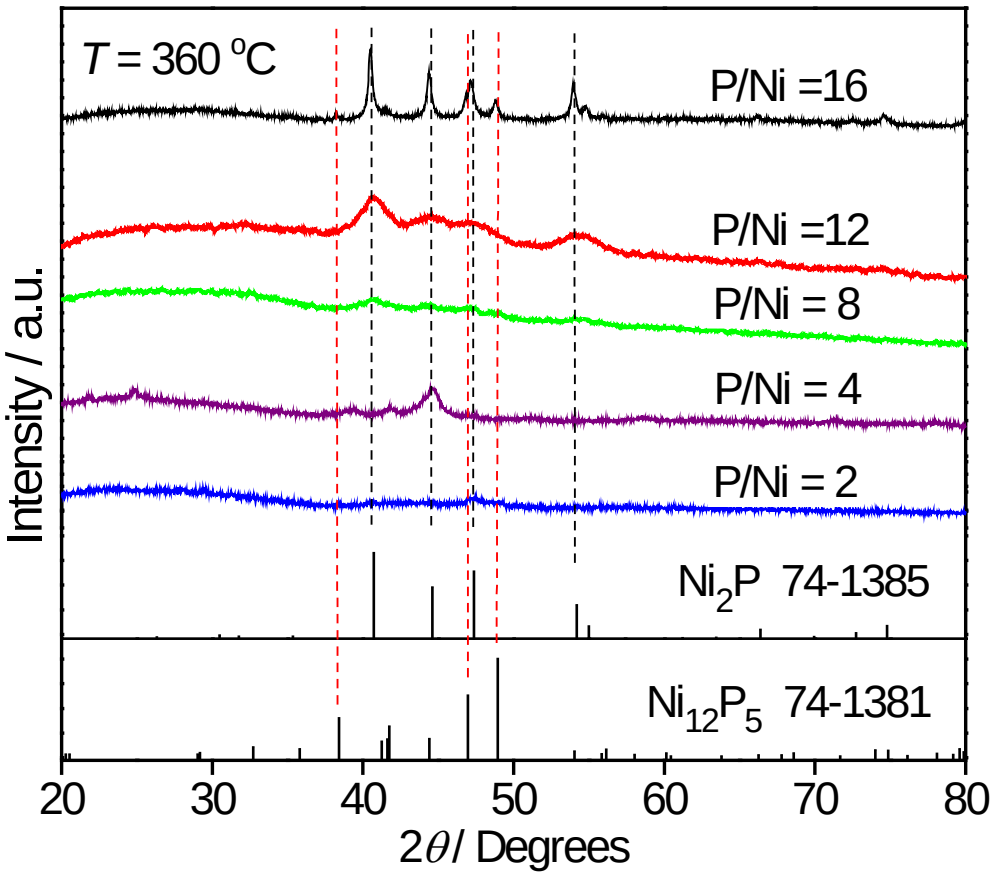

Figure 6. XRD patterns of Ni_2P nanoparticles synthesized with P/Ni ratio of 2 to 16; T = 360 °C; L = 1.0 mL/min; τ = 170 s; n_{Ni}= 1 mmol; $n_{1\text{-oct}}$ = 33 mmol. Reference patterns are also displayed (Ni_2P PDF # 74-1385; $Ni_{12}P_5$ PDF # 74-1381).

It is reported that during the synthesis of Ni_2P, Ni nanoparticles protected by oleylamine are formed as intermediate products. These Ni nanoparticles transform to hollow nickel phosphide nanoparticle when the temperature increased from 300 °C to 350 °C, as a result of the Kirkendall effect.[38] However, when the P/Ni ratio was greater than 2.8, the intermediate particles formed at 230 °C were amorphous Ni-P particles, and these produced fully dense nickel phosphide particles when the temperature

increased.[32] In our HCT, high P/Ni ratio is necessary for the formation of Ni_2P nanoparticles due to the short residence time. It can be seen from the XRD patterns of Figure6that higher P/Ni ratios result in the higher crystallinity of the product, which indicates that a higher P/Ni ratio is favorable for the crystallization of the nickel phosphide. This may have occurred because at short residence time, the nucleation and growth is completed and sufficient P atoms were present around the Ni atoms to facilitate the synthesis reaction. When P/Ni≥8, characteristic peaks at around $2\theta = 40.5^o$, 44.2^o, 46.8^o and 54.0^othat could be assigned to Ni_2P are observed. When P/Ni<8, peaks due to $Ni_{12}P_5$wasobserved, which indicate that the transformation to Ni_2P was incomplete.

3.2. Two-phases slug flow synthesis.

The previous results were obtained in single-phase mode. Due to the large size and impure phase of the Ni_2P particles prepared by the single-phase method, shorter residence times and more efficient mass transfer are required. Then the slug flow may be a good choice. This section reports the results of two-phases flow in plug flow reactor (PFR) mode in the HCT.

3.2.1. Synthesis of Ni_2P with different *G*/*L*.

Figure 7shows the photographs of two-phases flow in a HCT reactor

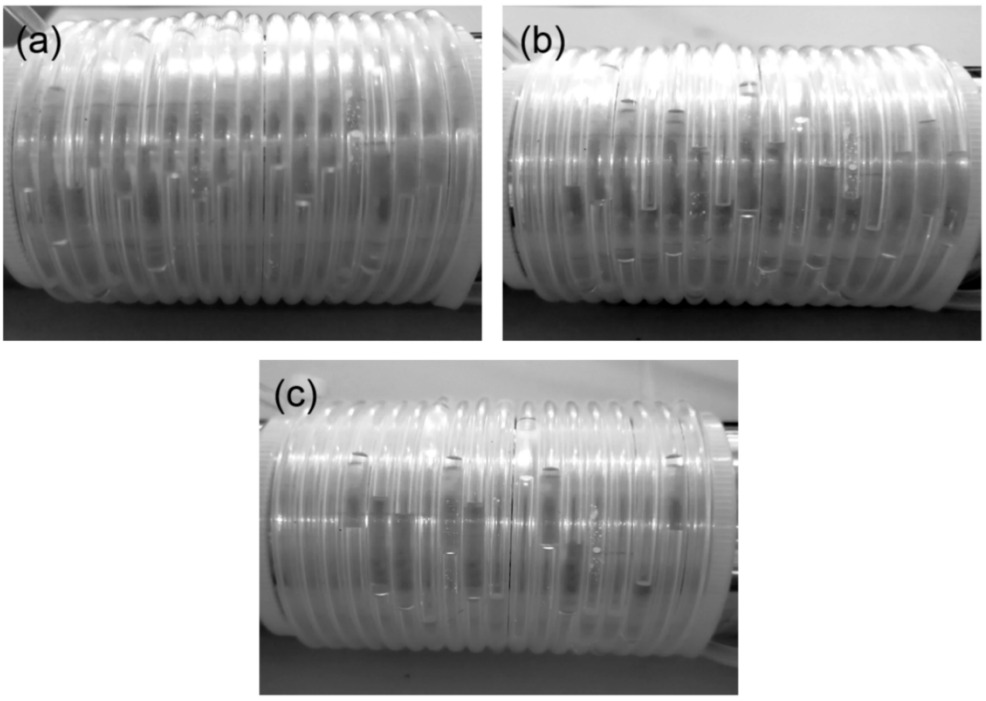

Figure 7. Photographs of slug flow in a HCT of d = 1.0 mm. (a) G = 1.0 mL/min; L = 0.5 mL/min; G/L = 2.0; (b) G = 0.5 mL/min; L = 1.0 mL/min; G/L = 0.5; (c) G = 0.5 mL/min; L = 0.5 mL/min; G/L = 1.0.

The flow is divided into liquid and gas segments, characteristic of slug flow. Three different gas (G) and liquid (L) flow rates were applied as indicated in Figure7. The corresponding residence times are calculated by Equation S2-2, and are reduced from

the nominal τ= 170 s to 77, 92, and 130 s, respectively (Table 3).

Table 3. Residencetime at 360 °C in the slug flow regime

G/L	τ / s	Particle size / nm
1.0/0.5 = 2.0	77	5.5
0.5/1.0 = 0.5	92	6.7
0.5/0.5 = 1.0	130	7.1

In the slug flow regime, the Ni_2P nanoparticles were synthesized inside the small liquid columns which were separated from each other by N_2 gas. Taylor- flow within the small liquid columns is reported to enhance rates of heat transfer, interfacial mass transfer as well as reaction rate. [39] An advantage of using this configuration is that the diffusion distance is short, so that the material mixing time is short according to the Einstein equation. For a diffusion coefficient of order 10^{-5} cm^2/s and a radius of 0.05 cm, this gives a characteristic time of τ = 250 s. In comparison, the residence time for the lengths of tubes used in this study were77– 130 s (Table 3). The reaction time is sufficient because there is mixing at a smaller scale than the radius.

It can be seen from the XRD pattern of the previous continuous flow experiments (Figure 4) that the prepared nanoparticles also containa$Ni_{12}P_5$ phase, which is caused by uneven concentration distribution and poor mixing in the single-phase flow in the milli-channel.[36]With the introduction of N_2 in the helical tube, the liquid phase flow converts to slug flow, which enhances the mass transfer and heat transfer and makes the liquid phase concentration more uniform. The concentration of the TOP solution in the liquid phase was 0.80 M at a reaction temperature of 360 °C and a bulk phase $Ni(acac)_2$ concentration of 0.05 M. The flow rate of the pumped liquid and the flow rate of the gas are indicated in Figure 7.

Figure 8 shows the XRD results of Ni_2P nanoparticles prepared continuously under different gas-liquid ratios (*G/L*).As shown in Figure 8, the crystal phase obtained in slug flow is mainly Ni_2P, and only a small peak at $2\theta = 48.8^o$ corresponding to the strongest peak of $Ni_{12}P_5$ is visible. Apparently, $Ni_{12}P_5$ is vastly reduced as compared to the case of continuous flow. This indicates that the slug flow formed by the addition of N_2 is beneficial to the formation of Ni_2P phase.

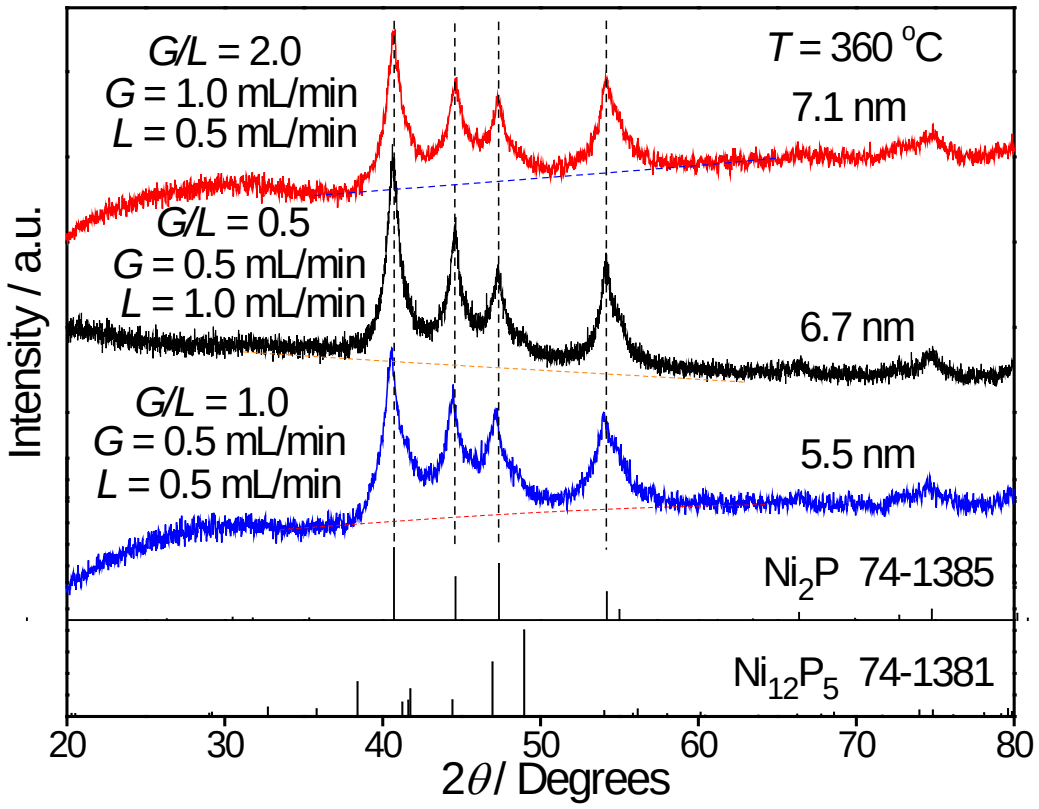

Figure 8. XRD patterns of Ni_2P nanoparticles synthesized in different gas and liquid flow rates; T = 360ºC; C_{Ni}=0.05 M; C_{TOP} = 0.80 M; $C_{1\text{-}oct}$ = 1.70 M. Reference patterns are also displayed (Ni_2P PDF # 74-1385; $Ni_{12}P_5$ PDF # 74-1381).

The three samples were further examined by TEM. The gas-liquid ratios (G/L) of the two-phases flow were2.0, 0.5 and 1.0, respectively, while the reaction temperature is 360 ºC and residence times are as shown in Table 3.All the Ni_2P nanoparticles prepared under the three conditions present close to monodisperse regular spherical morphology (Figure 9), and the particle size was 3-4 nm (Figure S6), which is considerably smaller than those obtained in single-phase system (28-42 nm, FiguresS3).

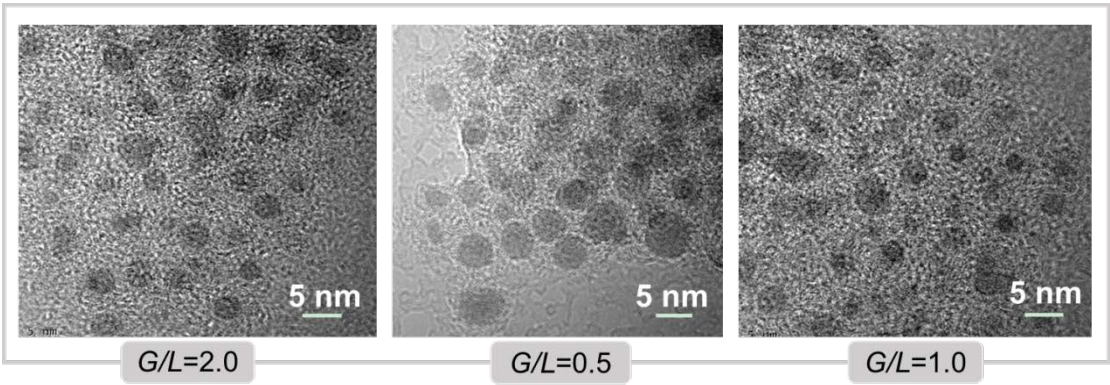

Figure 9. TEM micrographs of Ni_2P nanoparticles synthesized in different gas and liquid flow rates; T = 360 ºC; C_{Ni}=0.05 M; C_{TOP} = 0.80 M; $C_{1\text{-}oct}$ = 1.70M.

At the same time, it can be seen that the difference in the size of the Ni_2P nanoparticles produced with the different gas-liquid ratios is small. This may be ascribed to a more uniform residence time in the slug flow reactor. In comparison, the residence time distribution in laminar flow at continuous conditions is varied because the flow at the center is faster and there is limited mixing. Then the stability and repeatability of this method are further explored. Figure S7 and S8 show the results of repeated experiments with the same conditions, indicating that the obtained particles are similar in size and morphology, about 4nm.

The yields of Ni_2P prepared by slug flow at 320–360 ºC are listed in Table 4 and compared with those prepared by single-phase flow. And the product yield was calculated by the Equation S2-3. In both cases, the yield of Ni_2P increases with the increase of temperature. At the same temperature, the yields of Ni_2P prepared in the slug flow are much higher than those in the single-phase flow. Particularly, a high Ni_2P yield of 92% was achieved. This result combined with the results of XRD and TEM reveals that the slug flow is favorable for the production of Ni_2P nanoparticles. As shown in Figure 10, this may be explained as due to the presence of a secondary circulation flow in the liquid column of the slug flow in the spiral tube, which greatly strengthens the mass transfer process and makes the material concentration more uniform.

Table 4. Yield of Ni_2P prepared by slug flow and single-phase flow at different temperatures.

T/ºC[a]	Y/%	
	G-*L* two-phases (G = 0.5 mL/min, L = 0.5 mL/min)	*L* single-phase (L = 1.0mL/min)
320	82	77
340	85	78
360	92	81

[a]C_{Ni}=0.05 M; C_{TOP} = 0.80 M; $C_{1\text{-oct}}$ = 1.70 M.

3.2.2. Comparison between single-phase flow and slug flow in HCT.

On the basis of the above results, the slug flow is advantageous over the single-phase flow in the continuous preparation of Ni_2P.This is because different flow patterns have different mass transfer processes and effects.

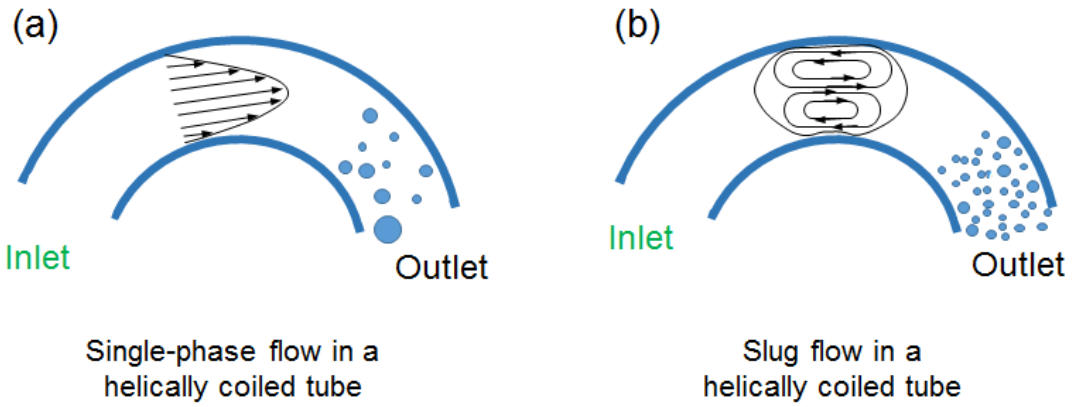

Figure 10. Flow patterns in helically coiled tube reactors. (a) Single-phase flow; (b) Slug flow.

In the case of continuous flow at laminar conditions, a parabolic velocity profile develops due to the viscous forces on the liquid phase which cause the shear stress near the tube wall to be larger. The actual flow in a helical reactor at laminar conditions has been analyzed [40] and results from a double vortex circulation superimposed on a parabolic profile. Despite the longer residence time in the laminar flow case the flow is segregated and mass transfer is limited. This results in lower overall reactant conversion, although the longer residence time results in larger particle sizes (Figure10a). In the case of slug flow, the liquid phase in the channel is divided into columns, and each column corresponds to an independent small reaction chamber, which accelerates the mixing speed of the material in the droplet. [37] The rate of nucleation is enhanced, but the limited residence time prevents growth of the particles, and as a result more smaller sized particles are formed. (Figure10b)

The results of this study show that nickel phosphide nanoparticles can be produced in high yield in the liquid phase in a continuous HCT reactor operated in plug flow mode. Compared with a traditional chemical system, the specific surface area of the fluid in the millifluidic reactor of dimensions ≤ 1 mm can reach the order of 10^4-10^6 m^2/m^3, due to the miniaturization of the internal channels and this can enhance heat transfer and lead to better control of the reaction temperature.[41] In a millifluidic reactor, internal circulation can also promote and ensure uniformity of the material distribution in the reactor, leading to enhanced reproducibility of the reaction process.[42]The results show that the interphase volumetric mass transfer coefficient in the millifluidic reactor can reach 10-1000 times that of traditional equipment,[43] and the interphase volumetric heat transfer coefficient can reach 10-50 times that of conventional equipment.[44]On the other hand, it is difficult to use batch reactor to prepare nano-catalyst for industrial amplification, but there is insignificant amplification effect in millifluidic reactor, which is conducive to the industrial production of nano-catalyst. When milli-reaction technology is used for production, the process amplification can be easily achieved by increasing the number of milli-channels rather than increasing the characteristic size of the milli-channel, and the time-consuming and laborious stage of intermediate stage tests amplification can be skipped.

4. Conclusions

In this study the synthesis of nickel phosphide in a continuous helical coil tube (HCT) reactor was studied at continuous liquid flow conditions and at slug flow conditions. The reactants were nickel acetylacetonate and tri-*n*-octylphosphine (TOP) in a 1-octadecene solvent. At continuous conditions, increasing reaction temperature from 320 to 360 ^{o}C promoted full conversion of the reagents to nickel phosphide but produced larger particles with a broad size distribution. Increasing TOP concentration from 0.60 to 1.0 M has little effect on the mean particle size, which was varied between 46 and 48 nm. Increasing the P/Ni ratio from 2 to 10 increased the amount of Ni_2P and a further increase to P/Ni = 16 enhanced the crystallinity of the product. Besides, increasing residence time did not form purer Ni_2P, suggesting that the reaction sequence was not just sequential but that an amorphous phase formed $Ni_{12}P_5$ before it was converted to Ni_2P. When the synthesis of nickel phosphide nanoparticles was conducted in a two-phases slug flow HCT reactor at 360 ^{o}C, an essentially pure Ni_2P phase with small crystallite size of 3-4 nm was formed. This was attributed to increased mass transfer in the small cells generated in the slugs. Compared with traditional synthetic methods, the preparation of nanoparticles using HCT is simple and easy to control. By precisely adjusting the reaction parameters, nanoparticles of different shapes and sizes can be prepared, which has extremely high controllability, and the growth mechanism of micro particles can also be studied. It also provides a reference for the continuous preparation of other nanoparticles.

Conflicts of interest

The authors declare no competing financial interest.

Acknowledgements

This work was supported by the National Natural Science Foundation of China (Grant 21706036), the Natural Science Foundation of Fujian Province (Grant 2018J05019), the Major Project on the Integration of Industry Education and Research of Fujian Province (Grants 2019H6010), the Special Project for Joint Innovation of Industrial Technology of Fujian Province (Grant FG-2016005), the Regional Development Project of Fujian Province (Grant 2016H4023), 111 Project (Project No. D17005) and the Program for New Century Excellent Talents in Fujian Province University (Grant HG2017-17). S. Ted Oyama is grateful for the Minjiang Scholar Visiting Professorship at Fuzhou University and support from the US Department of Energy, Office of Basic Energy Sciences, through Grant DE-FG02-963414669.

References

1 J. B.Edel, R. Fortt, J. C. Demello and A. J. Demello,*Chem. Commun.*, 2002, **10**(10), 1136-1137.
2 F. Pizzetti, V. M. A. Granata, U. Riva, F. Rossi and M.Masi, *React. Chem. Eng.*, 2019, **4**(10), 2117-2128.
3 G. R. Rippel, C. M. Eidt and H. B. Jordan, *Ind. Eng. Chem. Proc. Des. Dev.*, 1966, **5**(1), 32-39.
4 A. M. Nightingale and J. C. Demello, *Adv. Mater.*, 2013, **25**(13), 1813-1821.
5 S. E, Lohse, *Phys. Sci. Rev.*, 2018, **3**(31).
6 S. E. Lohse, J. R. Eller, S. T. Sivapalan, M. R. Plews and C. J. Murphy, *Acs. Nano.*, 2013, **7**(5), 4135-4150.
7 S. Biswas, J. T. Miller, Y. Li, K. Nandakumar and C. S. S. R. Kumar, *Small*, 2012, **8**(5), 688-698.
8 I. Shestopalov, J. D. Tice and R. F. Ismagilov, *Lab Chip*, 2004, **4**(4), 316-321.
9 M. Takagi, T. Maki, M. Miyahara and K. Mae, *Chem. Eng. J.*, 2004, **101**(1-3), 269-276.
10 Z. Liu, J. Zhu, C. Peng, T. Wakihara and T. Okubo, *React. Chem. Eng.*, 2019, **4**(10), 1699-1720.

11 M. N. Kashid, A. Renken and L. Kiwi-Minsker, *Chem. Eng. Sci.*, 2011, **66**(17), 3876-3897.
12 A. Günther, S. A. Khan, M. Thalmann, F. Trachsel and K. F. Jensen, *Lab Chip*,2004, **4**(4), 278-286.
13 I. Abuand K. Smith, *J. Catal.*, 2006, **241**(2), 356-366.
14 Q. Guan, W. Li, M. Zhang and K. Tao, *J. Catal.*, 2009, **263**(1), 1-3.
15 F. B. Wu, S. K. Tien, W. Y. Chen and J. G. Duh, *Surf. Coat. Technol.*, 2004, **177-178**, 312-316.
16 H. S. Yu, S. F. Luo and Y. R. Wang, *Surf. Coat. Technol.*, 2001, **148** (2-3), 143-148.
17 I. Lucas, L. Perez, C. Aroca, P. Sánchez, E. López and M. C. Sánchez, *J. Magn. Magn. Mater.*, 2005, **290-291**, 1513-1516.
18 J. A. Cecilia, A. Infantes-Molina, E. Rodríguez-Castellón and A. Jiménez-López, *J. Catal.*, 2009, **263**(1), 4-15.
19 P. Bui, J. A. Cecilia, S. T. Oyama, A. Takagaki, A. Infantes-Molina, H. Zhao, D. Li, E. Rodríguez-Castellón and A. Jiménez López, *J. Catal.*, 2012, **294**, 184-198.
20 J. Guan, Y. Wang, M. Qin, Y. Yang, X. Li and A. Wang, *J. Solid State Chem.*, 2009, **182**(6), 1550-1555.
21 X. Wang, P. Clark and S. T. Oyama, *J. Catal.*, 2002, **208**(2), 321-331.
22 Y.-K. Lee, Y. Shu and S. T. Oyama, *Appl. Catal., A*, 2007, **322**, 191-204.
23 S. Zhang, S. Zhang, L. Song and Q. Wei, *Powder Technol.*, 2014, **253**, 509–513.
24 S. Liu, X. Liu, L. Xu, Y. Qian and X. Ma,*J. Cryst. Growth*2007,**304**(2), 430-434.
25 K. Mi, Y. Ni and J. Hong, *J. Phys. Chem. Solids*, 2011, **72**(12), 1452-1456.
26 L. Mora-Tamez, G. Barim, C. Downes and R. L. Brutchey, *Chem. Mater.*, 2019, **31**, 1552−1560.
27 J. Park, B. Koo and K. Y. Yoon, *J. Am. Chem. Soc.*,2005, **127**, 8433-8440.
28 E. Muthuswamy, G. H. Layan Savithra and S. L. Brock, *ACS Nano* 2011, **5**(3), 2402-2411.
29 H.-R. Seo, K.-S. Cho and Y.-K. Lee, *Mater. Sci. Eng., B*, 2011, **176**(2), 132-140.
30 Y. Ni, A. Tao, G. Hu, X. Cao, X. Wei and Z. Yang, *Nanotechnology*,2006, **17** (19), 5013-5018.

31 S. E. Habas, F. G. Baddour, D. A. Ruddy, C. P. Nash, J. Wang, M. Pan, J. E. Hensley and J. A. Schaidle, *Chem. Mater.,* 2015, **27**(22), 7580-7592.
32 J.Zhang, K. Matsubara, G.-N. Yun, H. Zheng, A.Takagaki, R. Kikuchi and S. T. Oyama,*Appl. Catal., A,*2017, **548**, 39-46.
33 G. H. Layan Savithra, E. Muthuswamy, R. H. Bowker, B. A. Carrillo, M. E. Bussell and S. L. Brock, *Chem. Mat.,* 2013, **25**(6), 825-833.
34 S. Yang and R. Prins, *Chem. Commun. (Cambridge, U. K.),*2005, **36**(33), 4178-4180.
35 Y. Asano, S. Togashi, H. Tsudome and S. Murakami, *Pharm. Eng.,* 2010, 30(1), 1-9.
36 N. Guangda, R. Aleksey, V. Madeline and X. Younan, *Chem. Soc. Rev.,* 2015, **44**(16), 5806-5820.
37 M. Elayaraja, G. H. L. Savithra and S. L. Brock, *Acs Nano,* 2011, **5**(3), 2402-2411.
38 R.-K. Chiang and R.-T. Chiang, *Inorg. Chem.,* 2007, **46**(2), 369-371.
39 S. K. Kurt, M. G. Gelhausen and N. Kockmann, *Chem. Eng. Technol.,* 2015, **38**(7), 1122-1130.
40 D. M. Ruthven, *Chem. Eng. Sci.,*1971, **26**(7), 1113-1121.
41 W. Qu and I. Mudawar, *Int. J. Heat Mass Transfer,* 2003, **46**(15), 2755-2771.
42 S. Li, J. Xu, Y. Wang and G. Luo, *Chem. Eng. Sci.,*2007, **62**(13), 3620-3626.
43 Y. Zhao, G. Chen and Y. Quan, *AIChE J.,*2010, **53**(12), 3042-3053.
44 K. Wang, Y., C. Lu and H., W. Shao, *Ind. Eng. Chem. Res.,* 2008, **47**(23), 9754-9758.